High numerical aperture full-field optical coherence tomography with space-invariant resolution without scanning the focus

Daniel L. Marks[a], Tyler S. Ralston[a], P. Scott Carney[a],
and Stephen A. Boppart[a,b]

[a]Beckman Institute for Advanced Science and Technology and Department of Electrical and Computer Engineering University of Illinois at Urbana-Champaign, 405 N. Mathews, Urbana IL 61801

[b]Departments of Bioengineering and Medicine, University of Illinois at Urbana-Champaign, Urbana IL 61801

ABSTRACT

In high-numerical-aperture optical coherence tomography, the depth-of-field is usually quite short and therefore the focus is scanned through the object to form a well-resolved image of the entire volume. However, this may be inconvenient for *in vivo* scanning when precision placement is not easily achieved between the object and the focusing objective. We show that by scanning the illumination wavelength, and using novel inverse scattering methods on the detected interferograms, features outside of the focus can be resolved and therefore the focus does not need to be scanned.

Keywords: Optical coherence tomography, inverse scattering

The capabilities of optical coherence tomography (OCT)[1,2] and optical coherence microscopy[3–5] (OCM) have been greatly extended by computed imaging and synthetic aperture techniques.[6–9] Amongst the recently demonstrated advantages is the ability to resolve features in the sample that are outside of the confocal region. Ultimately a more quantitatively accurate and faithful representation of the sample structure is provided. In this work, by solving the inverse scattering problem[10] for full-field OCT/OCM,[11–20] we derive a novel variant where the focus remains fixed at the surface of the sample, and computed imaging techniques are used to infer the structure inside and outside of the depth-of-field. This variant obviates the requirement the focus be scanned through the sample.

Full-field OCT is capable of ranging an entire plane of scatterers simultaneously, which makes it a very rapid way to acquire the structure of a volume. A typical full-field OCT system consists of a Michelson interferometer with a broadband illumination source, from which reference and sample beams are derived. The sample is illuminated by a broadband collimated beam through a microscope objective, and the reference and backscattered sample signal are superimposed and focused on a CCD sensor which detects the interference signal. The amplitude of the interference signal corresponds to the reflections of scatterers at the focus plane. By translating the sample through the focus plane, the scatterers at many different depths may be ranged. While this method can be used to obtain high resolution images for entire volumes of a sample quickly, the sample and microscope objective must be translated relative to each other which is relatively slow and requires fine positioning.

We propose a method of full-field OCT that, instead of scanning the focus through the sample, the focus is fixed at the surface of the sample, and no relative translation is needed between the objective and the sample.

Further author information: (Send correspondence to S.A.B.)
S.A.B.: E-mail: boppart@uiuc.edu

Coherence Domain Optical Methods and Optical Coherence Tomography in Biomedicine XI
edited by James G. Fujimoto, Joseph A. Izatt, Valery V. Tuchin
Proc. of SPIE Vol. 6429, 64291R, (2007) · 1605-7422/07/$18 · doi: 10.1117/12.703372

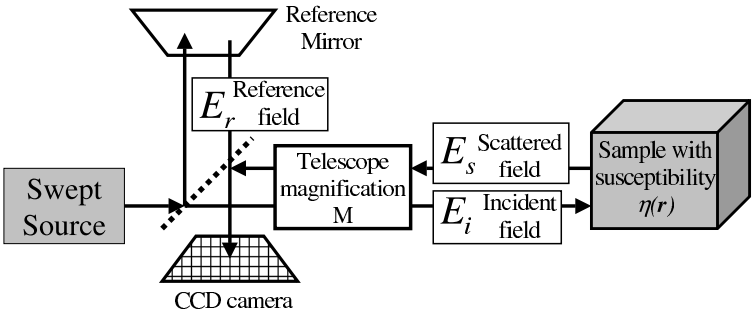

Figure 1. Diagram of full-field OCT using an afocal telescope to relay the field from the object to the CCD sensor plane.

A frequency-swept source can be utilized to provide a new degree of freedom, replacing information lost by fixing the focus, without sacrificing detail outside of the focus. Because the objective and sample can remain fixed relative to each other, no translation hardware is needed which makes placing the objective on a fiber optic or a handheld probe easier. This method may lead to faster and more accurate full-field OCT imaging because data acquisition can be very rapid, requiring only that the two-dimensional interferogram is sampled while the frequency of the source is scanned.

A diagram of the full-field OCT system being studied is in Fig. 1. This system is based on a Michelson interferometer, but other configurations such as a self-referencing Fizeau design could be used. In this system, the illumination source is a tunable narrow band laser. The laser is tuned to wavelengths λ that correspond to spatial frequencies $k = 2\pi/\lambda$. The laser nominally emits a plane wave (or is spatially filtered to produce one). The coherence length of this laser should be at least as twice as long as the total depth of the sample under study, to ensure there fields scattered throughout the entire sample simultaneously interfere with the reference field.

The laser illumination is split by a beam splitter into two components. One component travels to a reference mirror, and is reflected back through the beamsplitter to the output port where the focal plane array is located. The other component is demagnified by a factor $1/M$ using a telescope of magnification M. The purpose of the telescope is to concentrate the illumination onto the sample, and then relay a magnified scattered field to the focal plane array. This telescope consists of two converging lenses, a relay lens and a microscope objective. The illumination on the sample is a normally incident plane wave. The sample scatters some radiation backwards through the telescope. The telescope is aligned to afocally and telecentrically image the front surface of the sample to the focal plane array. Note that unlike standard full-field OCT microscopy, the focus of the objective remains fixed at the surface of the sample.

The object susceptibility, which is to be measured using OCT, is given by $\eta(\mathbf{r})$, and its three-dimensional Fourier transform $\tilde{\eta}(\mathbf{Q}) = \int\limits_V d^3r\ \eta(\mathbf{r}) \exp(i\mathbf{Q}\cdot\mathbf{r})$. If we define the data function $D(\mathbf{r};k) = E_r(\mathbf{r};k)^* E_s(\mathbf{r};k)$, the measured interference term between the reference and related sample fields, and the Fourier transform of this function is $\tilde{D}(\mathbf{q};k) = \int d^2r\ D(\mathbf{r};k) \exp(i\mathbf{q}\cdot\mathbf{r})$, the relationship between the measured data function and the object susceptibility $\eta(\mathbf{r})$ is given by

$$\tilde{D}(\mathbf{q};k) = \tilde{K}(\mathbf{q};k)\, \tilde{\eta}\left\{M\mathbf{q} + \hat{\mathbf{z}}\left[k + k_z(M\mathbf{q})\right]\right\}\ , \tag{1}$$

where the system bandpass function is defined

$$\tilde{K}(\mathbf{q};k) = M\, A(k)^2\, \tilde{P}(M\mathbf{q};k)\, k_z(M\mathbf{q})^{-1}\ . \tag{2}$$

where $k_z(\mathbf{q}) = \sqrt{k^2 - q^2}$, $A(k)$ is the amplitude of the illumination at frequency k, $\hat{\mathbf{z}}$ is the direction of increasing depth into the sample, the point spread function of the telescope is given by $P(\mathbf{r}; k)$, and its Fourier transform (the coherent transfer function of the telescope) is given by $\tilde{P}(\mathbf{q}; k) = \int d^2r \; P(\mathbf{r}; k) \exp(i\mathbf{q} \cdot \mathbf{r})$. This relation implies a correspondence between Fourier components of the data function and the object itself.

To demonstrate that three dimensional reconstruction can be achieved without scanning the focus through the volume, a simulation was performed. An object consisting of randomly placed point scatterers was imaged with a simulated full-field OCT system, and then the structure of the object was reconstructed from the data. The simulated object volume cross-sectional area was 25 wavelengths in depth, and 40 by 40 wavelengths in the transverse direction. The illumination source had a Gaussian spectrum with a 40% fractional full-width-half-max bandwidth (corresponding, for example, to 320 nm of bandwidth centered at 800 nm). The simulated numerical aperture of the imaging objective was 0.5.

Fig. 2, part (a) shows the projection of the simulated data collapsed (summed) along one transverse direction. The units are in terms of the center wavelength. Instead of showing the function $D(\mathbf{r}; k)$ itself, which would be difficult to interpret if it was plotted directly, we show the inverse Fourier transform of $D(\mathbf{r}; k)$ with respect to k. It is the data on the focal plane array that would be observed if the delay τ were scanned, rather than the frequency k. The focus is on the top surface at zero depth, which also corresponds to zero delay. As can be seen, as the delay is increased from zero, the diffracted images of the point scatterers become increasingly large. This corresponds to the standard degradation in resolution one expects from defocus when inverse scattering is not used.

To compute the image estimate $\eta^+(\mathbf{r})$ from the synthetic data $D(\mathbf{r}; k)$, first $\tilde{D}(\mathbf{q}; k)$ was computed using the two-dimensional Fourier transform. Next, the relation of Eq. (2) was used to infer $\tilde{\eta}^+ \{\mathbf{q} + \hat{\mathbf{z}}\,[k + k_z(\mathbf{q})]\}$. However, in practice to find $\eta^+(\mathbf{r})$ from $\tilde{\eta}^+(\mathbf{Q})$ numerically, one would likely use the three-dimensional inverse discrete Fourier transform. In practice, this means that the discrete sampling of the function $\tilde{\eta}^+$ is uniform in the variables $\mathbf{q}$ and k and not in $\mathbf{Q}$ to which the inverse Fourier transform can be directly applied. By using an interpolator, one can compute the samples of $\tilde{\eta}^+$ on points that are uniform in $\mathbf{Q}$ from existing samples of $\tilde{\eta}^\dagger \{\mathbf{q} + \hat{\mathbf{z}}\,[k + k_z(\mathbf{q})]\}$. In this simulation, a one-dimensional cubic B-spline interpolator was used to interpolate from the coordinates $\mathbf{q} + \hat{\mathbf{z}}\,[k + k_z(\mathbf{q})]$ to $\mathbf{Q}$. Because only the $\hat{\mathbf{z}}$ coordinate is not sampled uniformly, the resampling only needs to occur along this direction.

Finally, after taking the three-dimensional inverse Fourier transform of $\tilde{\eta}^+(\mathbf{Q})$, the reconstruction $\eta^+(\mathbf{r})$ results, which is shown in Fig. 2 part (b). Planes that are further from the focus have more diffuse images when viewed in the raw data because of the effect of defocus. One can also see the interference between the images of adjacent scatterers. Despite the interference between scatterers, each point is clearly resolved with space-invariant resolution in the reconstructed image. This shows the algorithm correctly separates the interference patterns from scatterers to produce high resolution images.

To demonstrate inverse scattering in frequency-scanned full-field OCT, we reconstructed a frequency-scanned full-field OCT system, imaged a test sample, and reconstructed the sample using the proposed method. To do so, we constructed a frequency-swept source by modifying a tunable continuous wave Ti-sapphire laser. This laser is a modified Spectra-Physics 3900S laser shown in Fig 3. The blue beam indicates the Argon-ion pump light and the red beam indicates the near-infrared light in the resonant laser cavity. This laser is tuned by rotating a birefringent filter, which is a birefringent plate placed at the Brewster's angle with respect to the beam orientation inside the cavity near the output coupler. By rotating the plate, the extraordinary axis of the filter is oriented differently with respect to the polarization of the mode of the Ti-sapphire cavity. Each wavelength will undergo a various phase retardance difference between the TE and TM polarizations with respect to the tuner surface normal. Only those wavelengths which have an unaltered polarization after passing through the tuner

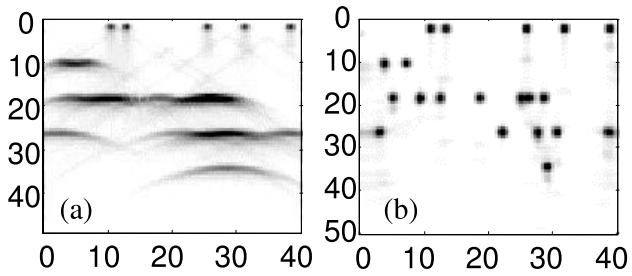

Figure 2. Simulation of reconstruction of the susceptibility of a collection of point scatterers using full-field optical coherence tomography without scanning the focus. Part (a) is the unprocessed interferometric data, part (b) is the image inferred by inverse scattering. The length dimensions of the axes are wavelengths.

will have the most gain, because the Brewster oriented surfaces do not reflect light for TM polarization. We have placed a motorized micrometer stage in place of the manual micrometer to allow a computer to automatically scan the wavelength of the laser. It was very important to orient the beam at the correct angle through the birefringent tuner, otherwise oscillations in the wavelength occurred as the wavelength was scanned.

A photograph of the interferometer that formed the full-field OCT setup is shown in Fig. 4. The beam is drawn in to help visualize the beam path. A beam expander telescope consisting of a 5 mm and 100 mm focal length converging achromats expands the laser beam to approximately 20 mm diameter. The expanded beam was divided into reference and sample portions by a near-infrared nonpolarizing beam splitter. The reference arm, which is the vertical arm in the photograph, was attenuated by double-passing through a pair of neutral density filters. A gold mirror on a translation stage was adjusted to delay the beam in the reference arm. This delay was set to match the delay from the beam splitter to the front of the sample surface in the sample arm.

In the sample arm, another telescope consisting of 200 mm and 50 mm converging near-infrared achromat lenses reduced the beam size by a factor of 4. This beam scatters from the sample. The sample consists of silicone polymer with embedded 20 μm-sized aluminum particles. A cover slip is adhered to the top of the sample with more transparent silicone to provide a flat surface. The surface reflection is reduced by turning the surface to an oblique angle relative to the beam. The sample beam is backscattered by the sample and recombined with the reference at the beamsplitter. A CCD camera detects the interference between the reference and sample signals. The CCD was placed so that the telescope afocally imaged the front surface of the sample onto the CCD surface.

Data acquisition consists of scanning the angle of the birefringent tuner to scan the wavelength of the laser, and acquiring two-dimensional interferograms on the camera. The camera array consists of 640x480 pixels at 7.4 μm pitch. Five hundred frames were acquired at 30 frames per seconds 10-bit resolution for a total of 300 MB of data. The approximate wavelengths scanned between were from 730-790 nm.

The data consisted of 512 interferograms of wavelength spaced 0.12 nm apart in wavelength. Because the laser does not scan the wavelength with uniform spacing in frequency, the data was resampled using a

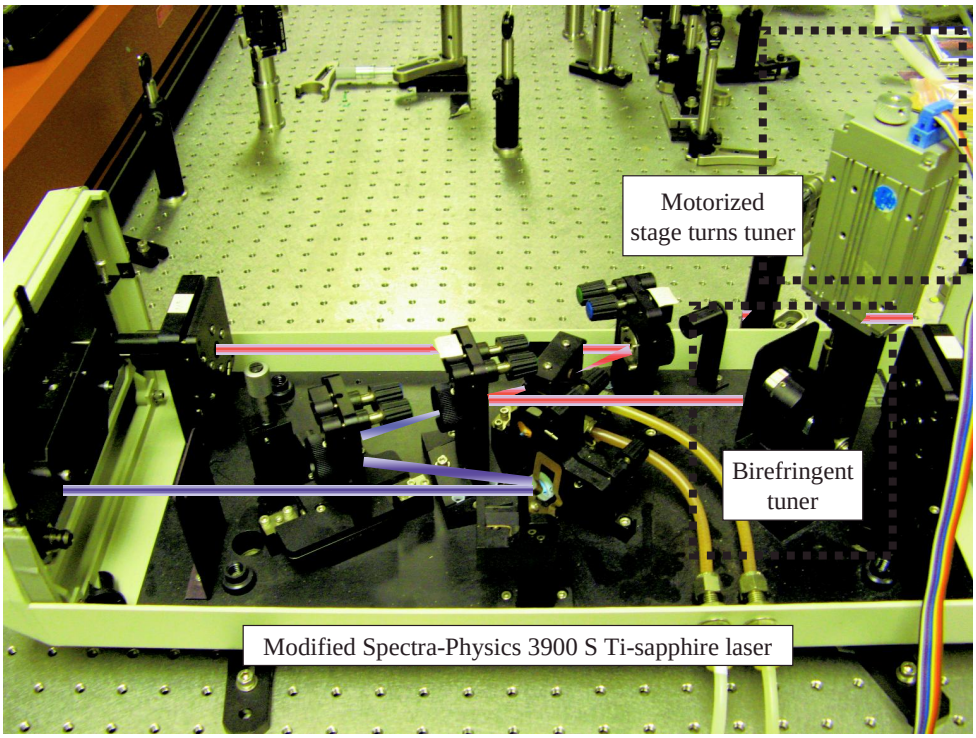

Figure 3. Photograph of Spectra-Physics 3900S tunable continuous-wave Ti-sapphire laser that is modified for automatic tuning of wavelength. A birefringent tuner is rotated to select the wavelength by motorized translation controlled by a computer. The beams are drawn into the setup to aid visualization of the operation of the laser.

combination of Fourier upsampling and cubic spline interpolation to produce a data set uniform in frequency by applying the laser tuning curve. The data was then inverse Fourier transformed with respect to frequency. The reconstructions of Fig. 5 result. The reconstructed points should be point-like, however, because defocus has not been compensated for, the images of the deeper points are more blurred.

To fix the defocus effect, we applied the resampling of Eq. 1 to the data. This consisted of taking the 3-D Fourier transform of the data to compute the Data set $\tilde{D}(\mathbf{q}; k)$. This data was resampled to be uniformly sampled in two new coordinates $\mathbf{Q}_{\|} = M\mathbf{q}$ and $\beta = \sqrt{k^2 - q^2}$, where M is the magnification of the telescope, in this case $M = 4$. The interpolator used to perform the resampling was a one-dimensional cubic-spline interpolator over the columns of constant $\mathbf{q}$. The resampling change the function to the sampled uniformly in β rather than k. After the resampling the inverse Fourier transform of the function $\eta(\mathbf{Q})$ is taken to recover the reconstructed volume accounting for defocusing.

The results of this procedure are shown in Fig. 6. The contrast of the image is better because the energy is better concentrated into the images of the pointlike scatterers, especially at deeper depths. The lateral blurring due to defocus is mostly absent from the properly reconstructed data.

As a further comparison, Fig. 7 shows three-dimensional isosurfaces plot of the magnitude of the 3-D reconstructed data before (a) and after (b) correction for defocus. Because the energy of the reconstructed volume without defocus correction is more spread out, the isosurface plot is more diffuse and has less well defined points. This is a defect not present in the defocus-corrected volume. This suggests that defocus correction is necessary to achieve resolution over the entire volume that full-field OCT is capable of.

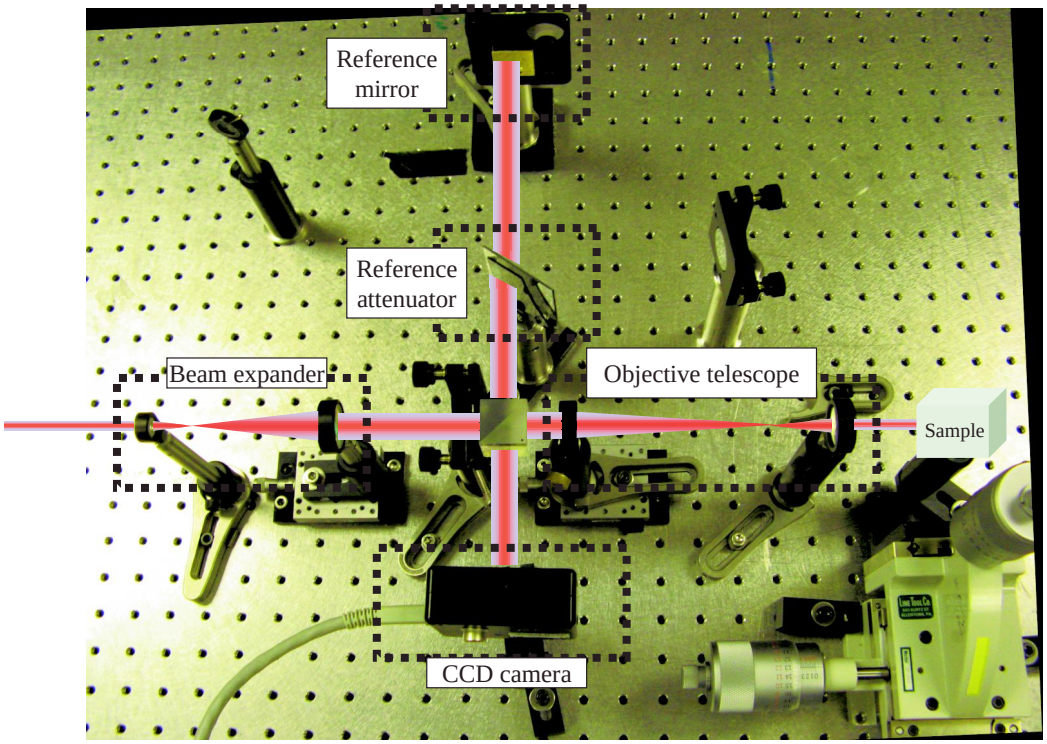

Figure 4. Photograph of full-field frequency-scanned OCT setup with parts labeled. The beams are drawn into the setup to aid visualization of the operation of the interferometer. On the left is a pair of lenses forming a beam expanding telescope. A beamsplitter in the middle splits the collimated beam into two parts. The part heading towards the top of the image is the reference beam. It is attenuated by a double-pass through two neutral-density filters and reflected off of a gold mirror. The other part is reduced by a telescope and illuminates the sample (drawn in). When the scattered light passes back through the telescope it is magnified. The reference and sample are recombined by the beamsplitter on the CCD camera (at the bottom).

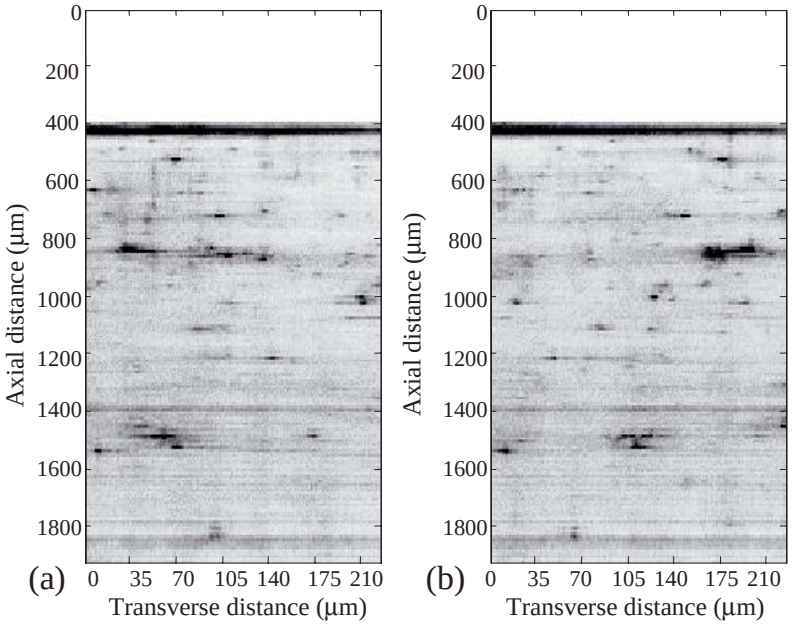

Figure 5. Computed projections of volume without resampling to account for diffraction. The object consists of aluminum point scatterers embedded in silicone. For larger depths, the images of the point scatterers becomes more blurred. Part (a) and (b) are orthogonal projections. All lengths are in microns.

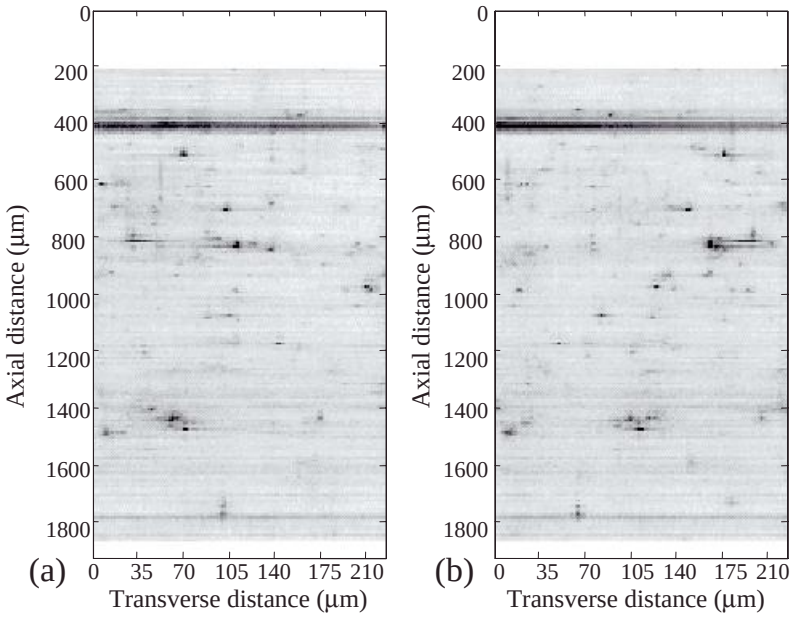

Figure 6. Computed projections of volume with resampling to account for diffraction. The scatterers are better defined and more-point like especially for larger depths. Part (a) and (b) are orthogonal projections. All lengths are in microns.

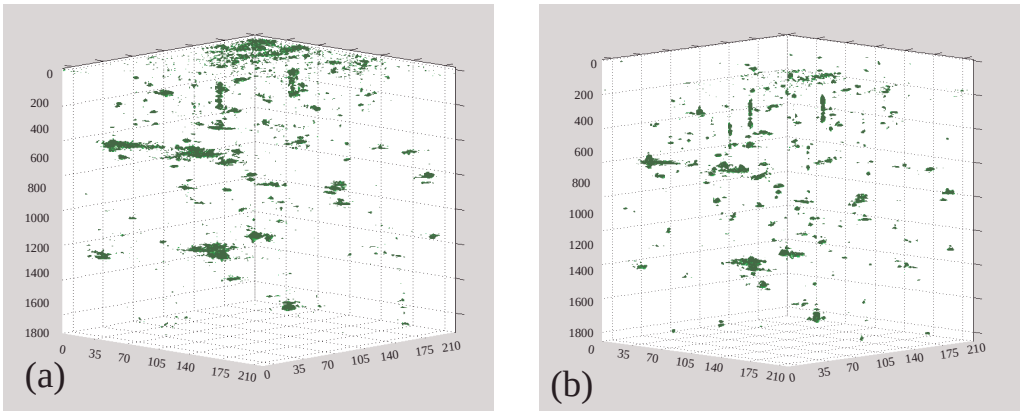

Figure 7. Three-dimensionally rendered isosurface plots of (a) the volume before diffraction correction and (b) the volume after diffraction correction. Because the energy is spread out more for the uncorrected version, the isosurface plots are also more spread out. The diffraction is corrected in part (b) to make the isosurfaces pointlike. All lengths are in microns.

1. ACKNOWLEDGEMENTS

We acknowledge Adam Zysk and Simon Schlacter for their help in setting up the laser, Joseph Matthesius for helping acquire the data, and Prof. Stephen Bishop for graciously allowing us to borrow his 3900S Ti-sapphire laser and modify it for our experiment.

REFERENCES

1. D. Huang, E. A. Swanson, C. P. Lin, J. S. Schuman, W. G. Stinson, W. Chang, M. R. Hee, T. Flotte, K. Gregory, C. A. Puliafito, and J. G. Fujimoto, "Optical Coherence Tomography," *Science* **254**(5035), pp. 1178–1181, 1991.
2. S. A. Boppart, B. E. Bouma, C. Pitris, J. F. Southern, M. E. Brezinski, and J. G. Fujimoto, "In vivo cellular optical coherence tomography imaging," *Nature Medicine* **4**, pp. 861–864, 1998.
3. J. A. Izatt, M. R. Hee, G. M. Owen, E. A. Swanson, and J. G. Fujimoto, "Optical coherence microscopy in scattering media," *Opt. Lett.* **19**, pp. 590–592, 1994.
4. J. M. Schmitt, M. J. Yadlowsky, and R. F. Bonner, "Subsurface imaging of living skin with optical coherence microscopy," *Dermatology* **191**, pp. 93–98, 1995.
5. J. A. Izatt, H.-W. Kulkarni, K. Wang, M. W. Kobayashi, and M. W. Sivak, "Optical coherence tomography and microscopy in gastrointestinal tissues," *IEEE J. Selected Topics in Quantum Elect.* **2**, pp. 1017–1028, 1996.
6. T. S. Ralston, D. L. Marks, P. S. Carney, and S. A. Boppart, "Inverse scattering problem for optical coherence tomography," *J. Opt. Soc. Am. A* **23**, pp. 1027–1037, 2006.
7. T. S. Ralston, D. L. Marks, S. A. Boppart, and P. S. Carney, "Inverse scattering for high-resolution interferometric microscopy," *Opt. Lett.* **24**, pp. 3585–3587, 2006.
8. T. S. Ralston, D. L. Marks, P. S. Carney, and S. A. Boppart, "Interferometric synthetic aperture microscopy," *Nature Phys.* **in press**, 2007.
9. D. L. Marks, T. S. Ralston, P. S. Carney, and S. A. Boppart, "Inverse scattering for rotationally scanned optical coherence tomography," *J. Opt. Soc. Am. A* **23**, pp. 2433–2439, 2006.

10. D. L. Marks, T. S. Ralston, P. S. Carney, and S. A. Boppart, "Inverse scattering for frequency-scanned full-field optical coherence tomography," *J. Opt. Soc. Am. A* **in press**, 2007.
11. E. Beaurepaire and A.-C. Boccara, "Full-field optical coherence microscopy," *Opt. Lett.* **23**, pp. 244–246, 1998.
12. A. Dubois, L. Vabre, A.-C. Boccara, and E. Beaurepaire, "High-resolution full-field optical coherence tomography with a Linnik microscope," *Appl. Opt.* **41**, pp. 805–812, 2002.
13. A. Dubois, K. Grieve, G. Moneron, R. Lecaque, L. Vabre, and C. Boccara, "Ultrahigh-resolution full-field optical coherence tomography," *Appl. Opt.* **43**, pp. 2874–2883, 2004.
14. A. Dubois, G. Moneron, K. Grieve, and A.-C. Boccara, "Three-dimensional cellular-level imaging using full-field optical coherence tomography," *Phys. Med. Biol.* **49**, pp. 1227–1234, 2004.
15. K. Grieve, A. Dubois, M. Simonutti, M. Paques, J. Sahel, J.-F. Le Gargasson, and C. Bocarra, "In vivo anterior segment imaging in the rat eye with high speed white light full-field optical coherence tomography," *Opt. Expr.* **13**, pp. 6286–6295, 2005.
16. B. Laude, A. De Martino, B. Drevillon, L. Benattar, and L. Schwartz, "Full-field optical coherence tomography with thermal light," *Appl. Opt.* **41**, pp. 6637–6645, 2002.
17. G. Moneron, A.-C. Bocarra, and A. Dubois, "Stroboscopic ultrahigh-resolution full-field optical coherence tomography," *Opt. Lett.* **30**, pp. 1351–1353, 2005.
18. J. Moreau, V. Lorlette, and A.-C. Bocarra, "Full-field birefringence imaging by thermal-light polarization-sensitive optical coherence tomography. II. instrument and results," *Appl. Opt.* **42**, pp. 3811–3818, 2003.
19. Y. Watanabe, Y. Hayasaka, M. Sato, and N. Tanno, "Full-field optical coherence tomography by achromatic phase shifting with a rotating polarizer," *Appl. Opt.* **44**, pp. 1387–1392, 2005.
20. B. Povazay, A. Unterhuber, B. Hermann, H. Sattmann, H. Arthaber, and W. Drexler, "Full-field time-encoded frequency-domain optical coherence tomography," *Opt. Express* **14**, pp. 7661–7669, 2006.